

16. Sciagra R, Bisi G, Buonamici P, et al. Left ventricular cavity-to-myocardium count ratio in technetium-99m-sestamibi SPECT in the detection of patients with resting left ventricular dysfunction. *J Nucl Med* 1997;38:766-770.
17. Picano E, Marzullo P, Gigli G, et al. Identification of viable myocardium by dipyridamole-induced improvement in regional left ventricular function assessed by echocardiography in myocardial infarction and comparison with thallium scintigraphy at rest. *Am J Cardiol* 1992;70:703-710.
18. Schiller NB, Shah PM, Crawford M, et al., for the American Society of Echocardiography Committee of Standards, Subcommittee on Quantification of Two-Dimensional Echocardiography. Recommendation for quantification of the left ventricle by two-dimensional echocardiography. *J Am Soc Echocardiogr* 1989;5:358-367.
19. Baer FM, Voth E, Deutsch HJ, Schneider CA, Schicha H, Sechtem U. Assessment of viable myocardium by dobutamine transesophageal echocardiography and comparison with fluorine-18 fluorodeoxyglucose positron emission tomography. *J Am Coll Cardiol* 1994;24:343-353.
20. Perrone-Filardi P, Pace L, Prastaro M, et al. Dobutamine echocardiography predicts improvement of hypoperfused dysfunctional myocardium after revascularization in patients with coronary artery disease. *Circulation* 1995;91:2556-2565.
21. Hanley JA, McNeil BJ. The meaning and use of the area under a receiver operating characteristic (ROC) curve. *Radiology* 1982;143:29-36.
22. Afifi AA, Clark V. Discriminant analysis. In: *Computer-aided multivariate analysis*. New York: Von Nostrand Company; 1984:246-286.
23. Hanley JA, McNeil BJ. A method of comparing the areas under receiving operating characteristic curves derived from the same cases. *Radiology* 1983;148:839-843.
24. Kiat H, Berman DS, Maddahi J, et al. Late reversibility of tomographic myocardial thallium-201 defects: an accurate marker of myocardial viability. *J Am Coll Cardiol* 1988;12:1456-1463.
25. Dilsizian V, Rocco TP, Freedman NM, Leon MB, Bonow RO. Enhanced detection of ischemic but viable myocardium by the reinjection of thallium after stress-redistribution imaging. *N Engl J Med* 1990;323:141-146.
26. Ingelse E, Brambilla M, Dondi M, et al. Assessment of myocardial viability after thallium-201 reinjection or rest-redistribution imaging: a multicenter study. *J Nucl Med* 1995;36:555-563.

## Impairment of BMIPP Uptake Precedes Abnormalities in Oxygen and Glucose Metabolism in Hypertrophic Cardiomyopathy

Eiji Tadamura, Takashi Kudoh, Naoya Hattori, Masayuki Inubushi, Yasuhiro Magata, Junji Konishi, Akira Matsumori, Ryuji Nohara, Shigetake Sasayama, Muneo Yoshibayashi and Nagara Tamaki  
 Departments of Nuclear Medicine, Internal Medicine (Third Division) and Pediatrics, Kyoto University Faculty of Medicine, Kyoto; and Department of Nuclear Medicine, Hokkaido University School of Medicine, Sapporo, Japan

Impairment of fatty acid uptake is shown to precede myocardial perfusion abnormality using  $^{123}\text{I}$ -labeled 15-(*p*-iodophenyl)-3-(*R,S*)-methylpentadecanoic acid (BMIPP) in an experimental model of hypertrophic cardiomyopathy (HCM) and in human studies. We have recently demonstrated that abnormalities of both glucose and oxidative metabolism precede the reduction of blood flow in HCM. The main purposes of this study were to assess the frequency of abnormal findings in FDG uptake, BMIPP uptake and oxygen metabolism and to clarify the relationship among these metabolic parameters by using PET and SPECT. **Methods:** Twenty-eight subjects with HCM underwent FDG- and acetate-PET and thallium- and BMIPP-SPECT studies at rest, respectively. After correcting for partial volume effect, real percentages of FDG and BMIPP uptake were calculated. In addition, the clearance rate constant ( $K_{\text{mono}}$ ) of acetate was measured and normalized (%) to estimate the oxygen metabolism. **Results:** There were various metabolic abnormalities observed in patients with HCM. BMIPP uptake was often impaired without significant reduction of  $K_{\text{mono}}$  values or FDG uptake. Thus, abnormality of BMIPP uptake was more frequently observed than that for FDG uptake or  $K_{\text{mono}}$  values ( $p < 0.0001$ , respectively). FDG uptake was relatively maintained even in the segments with reduced  $K_{\text{mono}}$  values and reduced BMIPP uptake. **Conclusion:** HCM shows a variety of metabolic patterns; however, the results of our study suggest that reduction of BMIPP uptake appears to be the most sensitive indicator of metabolic abnormalities followed by reduction of oxidative metabolism in patients with HCM.

**Key Words:** hypertrophic cardiomyopathy; BMIPP; PET; glucose metabolism; oxidative metabolism

**J Nucl Med** 1998; 39:390-396

The heart muscle can metabolize a variety of substrates including free fatty acids, glucose, lactate, pyruvate, ketone bodies and amino acids, depending on plasma substrate levels, hormonal conditions and oxygen availability (1-4). In the fasting state, oxidation of fatty acids is the important source of myocardial energy production. Long-chain fatty acids are known to account for approximately 70% of myocardial energy production while carbohydrates provide the majority of the remaining 30% of energy requirements (1,3). After carbohydrate loading, on the other hand, the myocardium utilizes glucose as a primary energy source as a result of the change in metabolic conditions. While the assessment of myocardial metabolism may be complicated by this diversity, it may lead to unique patterns of substrate utilization that reflect cardiac pathophysiology. Identification of these patterns using various metabolic tracers may contribute to our understanding of the pathophysiology in a variety of cardiac diseases (5,6).

Alterations in the metabolism of glucose and free fatty acid have been reported using PET and SPECT in patients with hypertrophic cardiomyopathy (HCM) (7-12). Sochor et al. (7) demonstrated inhomogeneous uptake of  $^{11}\text{C}$  palmitate in the hypertrophic myocardium and delayed clearance from the myocardium in a small number of patients. Grover-McKay et al. (8) have shown the reduced uptake of FDG and free fatty acids using PET. Impaired regional fatty acid utilization has also been demonstrated using  $^{123}\text{I}$ -labeled 15-(*p*-iodophenyl)-3-(*R,S*)-methylpentadecanoic acid (BMIPP), a radiolabeled long-chain fatty acid analog (13,14) in an experimental model of HCM (9) and in human studies (10-12).

Using PET, we have recently demonstrated that not only glucose but also oxidative metabolism were sometimes impaired in the hypertrophic myocardium, while the resting myocardial perfusion was not significantly changed (15). It is still unknown which metabolic alterations may precede the

Received Jan. 16, 1997; revision accepted Apr. 15, 1997.

For correspondence or reprints contact: Eiji Tadamura, MD, Department of Nuclear Medicine and Diagnostic Imaging, Kyoto University Faculty of Medicine, 54 Shogoin Kawahara-cho, Sakyo-ku, Kyoto, 606-01, Japan.

other in patients with HCM. To clarify the relationship of oxidative metabolism, FDG uptake and BMIPP uptake, and to assess the frequency of the abnormality of these parameters, combined PET imaging using FDG and  $^{11}\text{C}$ -acetate, and SPECT imaging using thallium and BMIPP were performed in the same patients.

## MATERIALS AND METHODS

### Subjects

This study group consisted of 28 patients (16 men, 12 women; age range 13–82 yr; mean age 43.9 yr). HCM was defined as hypertrophied and nondilated left ventricle in the absence of any other cardiac or systemic disease that itself produces left ventricular hypertrophy (16,17). The diagnosis of HCM was made based on the clinical course and results of echocardiography, electrocardiography, MRI and left ventriculography. No patient had a history of diabetes or hypertension. Each subject gave written informed consent approved by the Kyoto University Ethics Committee.

### Echocardiographic Studies

Echocardiographic studies were performed with an HP model 1000 instrument (Hewlett-Packard Co., Palo Alto, CA) using 2.5- and 3.5-MHz transducers. M-mode echocardiography was performed on parasternal long- and short-axis views and apical two- and four-chamber views. The M-mode echocardiographic measurements were performed according to the criteria recommended by the American Society of Echocardiography (18).

When the end-diastolic thickness of the septum was at least 15 mm and its ratio to that of the left ventricular posterior wall was 1.3 or greater, asymmetrical septal hypertrophy was considered to be present (10). When the echocardiographic apical long axis or four-chamber view demonstrated apical hypertrophy and a spade-like configuration was also found in the right anterior oblique ventriculogram at end-diastole, apical hypertrophy was considered to be present (19).

Hypertrophy of the anterior septum or the posterior free wall was assessed as present when diastolic wall thickness was  $\geq 15$  mm; hypertrophy of the posterior septum and lateral free wall was defined as a diastolic thickness  $\geq 17$  mm (20,21).

### SPECT Imaging

SPECT was performed 20 min after injection of 111 MBq (3 mCi)  $^{123}\text{I}$ -BMIPP at rest after overnight fasting. SPECT images were obtained with a rotating gamma camera equipped with a low-energy, general-purpose collimator, collecting 32 views, 30 sec each, over  $180^\circ$  from the right anterior oblique to the left posterior oblique projections. The total acquisition time was approximately 18 min (22).

Thallium SPECT imaging was performed on a separate day. After injection of 100 MBq (2.7 mCi) of thallium at rest, SPECT images were obtained 15 min later in a similar manner as the BMIPP study.

After tomographic acquisition, each projection was stored on a hard disk and smoothed with a Hanning filter with a cutoff frequency of 0.5 cycle per pixel. A series of transverse slices of 6-mm thickness per slice were reconstructed by use of a filtered backprojection technique with a ramp filter (23). The in-plane resolution of the SPECT scanner was 16-mm at full width half maximum (FWHM) after reconstruction. Data were reoriented to obtain the oblique-angle tomograms parallel to the long-axis of the left ventricle. No attenuation or scatter correction was performed. SPECT imaging using both thallium and BMIPP was performed in 22 subjects of this study group.

### PET Imaging

The PET studies were performed using a whole-body PET camera (PCT 3600W, Hitachi Medical Co., Tokyo, Japan), providing 15 slices simultaneously at 7-mm intervals. The scanner has an effective resolution of 9 mm and an axial resolution of 7 mm at FWHM after reconstruction (22,24,25). Each subject was positioned in the gantry of the PET camera with the aid of ultrasound. At the beginning of the PET study, a transmission scan was obtained for 20 min using a  $^{68}\text{Ge}/^{68}\text{Ga}$  external source to correct photon attenuation.

Approximately 185 MBq (5 mCi) of FDG was administered at rest 40–60 min after a 75-g oral glucose load. Serial dynamic PET scans (30 sec  $\times$  8 frames, 4 min  $\times$  12 frames) were performed after FDG administration. FDG-PET imaging was performed in 23 subjects of this study group.

On a different day, serial PET imaging was performed at rest after infusion of 370 MBq (10 mCi)  $^{11}\text{C}$ -acetate acquiring 20 frames of 60 sec each for 20 min to assess oxidative metabolism and perfusion (22,26). Acetate PET studies were conducted in 24 subjects of the study group. All of the PET and SPECT studies were performed within 5 wk.

### Data Analysis

**SPECT Data.** Eleven regions of interest (ROI) were drawn on the thallium and BMIPP transaxial images in a similar fashion to assess apparent regional thallium and BMIPP uptake (25). Our previous investigations using PET have shown that myocardial blood flow after correction for partial volume effect is approximately homogenous throughout the myocardium (15). The spatial resolutions of PET and SPECT scanner are different. Therefore, BMIPP uptake was corrected for partial volume effect, using thallium perfusion images. BMIPP uptake was measured as 100% in the nonhypertrophic posterior segment of the midventricular slice to obtain the normalized apparent BMIPP uptake. Similarly, data for apparent perfusion were normalized (%). To obtain the normalized real BMIPP uptake without partial volume effect, the real percentage of regional BMIPP uptake in each ROI was calculated as follows:

Real percentage of regional BMIPP uptake

$$= (\% \text{ apparent BMIPP-uptake}) / (\% \text{ apparent thallium uptake}) \times 100.$$

Eq. 1

**PET Data.** PET perfusion images were reconstructed from the frame with the peak myocardial activities in the dynamic acetate images (15,22,27). FDG static images were reconstructed from the last three frames (between 40 and 52 min postinjection) (15). These PET images represent apparent regional perfusion and FDG uptake including partial volume effect. After reconstruction of 15 slices of transverse tomograms, oblique tomograms parallel to the long-axis of the left ventricle were also reconstructed. Eleven ROIs were drawn on the corresponding three transaxial images in the apparent perfusion and FDG images in a similar fashion. In the analysis of FDG-PET and PET-perfusion images, apparent FDG uptake and PET-perfusion were measured as 100% in the nonhypertrophic posterior segment of the midventricular slice. Like in the analysis of BMIPP SPECT images, the real percentage of regional FDG uptake in each ROI was calculated as 100% in the nonhypertrophic posterior segment of the midventricular slice using the following equation:

Real percentage of regional FDG uptake

$$= (\% \text{ apparent-FDG-uptake}) / (\% \text{ apparent-perfusion}) \times 100. \quad \text{Eq. 2}$$

In the analysis of  $^{11}\text{C}$ -acetate PET studies, the time-activity curves of the corresponding 11 ROIs were generated from serial

PET images after correction of dead time, physical decay and cross contamination (26–28). From these time-activity curves, the clearance rate constant (K mono) (/min) of each ROI was calculated by a monoexponential fitting as a marker of oxidative metabolism (22,26,29,30). Theoretically, K mono values are not affected by partial volume effect. K mono values were also normalized as 100% in the posterior segment of the midventricular slice. K mono images were also created by calculating the clearance rate constant pixel-by-pixel in a similar fashion. After reconstruction of 15 slices of transverse K mono images, oblique tomograms parallel to the horizontal long-axis of the left ventricle were also reconstructed for the display purpose.

The frequency of abnormal segments was analyzed for BMIPP uptake, FDG uptake and oxidative metabolism in the 17 subjects who underwent every study. The uptake of FDG or BMIPP was considered to be impaired when the real percentage of these tracers was < 80%. Similarly, oxidative metabolism was judged as abnormal if the K mono value was < 80%. The borderline of 80% was determined by our observation of the metabolic parameters in the nonhypertrophic myocardium. The mean value minus 2 s.d., i.e., 80% was chosen as the lower normal limit (Table 1).

### Statistical Analysis

Data were presented as mean  $\pm$  s.d. To compare the frequency of the abnormal segments of BMIPP uptake, FDG uptake and K mono values, chi-square analysis was performed. Comparison of myocardial metabolic parameters was performed by unpaired Student's t-test (between two groups) or analysis of variance with posthoc Scheffé's F-test (among three groups). Significant differences were considered to be present when p value was < 0.05.

## RESULTS

Table 2 summarizes the patients' profiles and the results of ultrasonography and scintigraphy.

### Frequency of Abnormality

Abnormality of BMIPP uptake was observed in 15 subjects (72.7%) among the 22 subjects who underwent SPECT imaging. Reduction of K mono values was noted in 11 (45.8%) of 24 subjects who underwent acetate PET studies, while abnormality of FDG uptake was seen in 6 (26.1%) of 23 patients in whom FDG-PET imaging was performed.

Abnormal segments of BMIPP uptake (33.7%) were more frequently observed than those of FDG uptake (5.3%) or K mono values (18.2%) in patients with HCM ( $p < 0.0001$ , respectively). The frequency of abnormal segments of K mono values was more than that of FDG uptake ( $p = 0.0001$ ).

### Real BMIPP Uptake and Real FDG Uptake Versus K Mono Value

Table 1 shows the results of metabolic parameters in the hypertrophic and nonhypertrophic segments. Every metabolic parameter was lower in the hypertrophic myocardium than in the nonhypertrophic myocardium ( $p < 0.0001$ ). In the nonhypertrophic myocardium, the three metabolic parameters did not differ significantly. In the hypertrophic myocardium, on the other hand, real percentage of BMIPP uptake was significantly lower than that of FDG uptake and percent K mono ( $p < 0.0001$ , respectively). In addition, percent K mono was also significantly lower than real percentage of FDG uptake ( $p = 0.0088$ ).

Figure 1 shows the relationship between the real percentage of BMIPP uptake and the percent K mono values in 18 subjects who underwent both acetate-PET and SPECT studies. Figure 2 shows the relationship between the real percentage of FDG uptake and the percent K mono values in 17 subjects who underwent both FDG-PET and SPECT studies. These figures

**TABLE 1**  
Results of Metabolic Parameters in Hypertrophic and Nonhypertrophic Myocardium

	Hypertrophic	Nonhypertrophic
Real percentage of FDG uptake	90.9 $\pm$ 12.3 <sup>†</sup>	96.5 $\pm$ 7.9
Real percentage of BMIPP uptake	73.1 $\pm$ 16.1	95.6 $\pm$ 7.6
Percent K mono	85.2 $\pm$ 15.2 <sup>‡</sup>	96.2 $\pm$ 7.9

<sup>†</sup> $p < 0.0001$  vs. real percentage of BMIPP uptake.  
<sup>‡</sup> $p = 0.0088$  vs. percent K mono.  
<sup>†</sup> $p < 0.0001$  vs. real percentage of BMIPP uptake.

indicate that FDG uptake was always maintained when the K mono values were normal. However, there were two types of segments including those with normal BMIPP uptake (Fig. 3) and those with reduction of BMIPP uptake (Fig. 4). Among those with reduction of K mono values, some segments showed reduced BMIPP uptake with relatively preserved FDG uptake (Fig. 5). When the reduction of K mono values was severe, FDG uptake was also reduced as well as BMIPP uptake (Fig. 6).

## DISCUSSION

The present data demonstrate that a variety of metabolic patterns are present in HCM. Among them, reduction of BMIPP uptake was more frequently observed than the impairment of FDG uptake and oxidative metabolism, suggesting that impairment of long-chain fatty acid metabolism may precede other metabolic abnormalities in the hypertrophic myocardium.

### Correction for Partial Volume Effect

Quantitative assessment of HCM by radionuclide imaging is always hampered by low spatial resolution. The partial volume effect causes underestimation of regional tissue activities when the thickness of the myocardial wall is less than twice the spatial resolution of the imaging device (31). Asymmetrical hypertrophy of left ventricular myocardium is characteristic in HCM. The partial volume effect causes underestimation of the true count especially in the nonhypertrophic myocardium. Therefore, an appropriate correction for this effect is required for the assessment of the true tracer concentrations, using recovery coefficient and anatomical information obtained by ultrasonography or MRI (8,15,21). We have recently demonstrated that the resting myocardial blood flow after correction for partial volume effect is approximately homogenous throughout the myocardium in patients with HCM (15). Therefore, we used perfusion images (acetate images with peak myocardial activities or thallium images) to correct for this effect. Myocardial glucose and oxidative metabolism are considered to be normal in the nonhypertrophic myocardium (15). Moreover, BMIPP uptake is reported to be impaired in the hypertrophic myocardium (9–12). Therefore, we have normalized these parameters to the nonhypertrophic myocardium.

### Mechanism of BMIPP Uptake

Iodine-123-BMIPP is a methyl-branched long-chain fatty acid analog. Because of rapid clearance of the blood activity and long tracer retention in the myocardium after BMIPP administration, excellent images of the ventricular myocardium are obtained, particularly with SPECT (32,33). Most BMIPP is trapped in the triglyceride fraction, and a small percentage of BMIPP is catabolized by initial  $\alpha$ -oxidation in the cells (34,35). The myocardial uptake of BMIPP is affected by regional blood flow, a decreased triglyceride pool, and increased back diffusion from cells because of reduced ATP (34,35). We have also demonstrated that BMIPP uptake does not reflect  $\beta$ -oxidation

**TABLE 2**  
Patient Profiles and the Results of Echocardiography and Scintigraphy

Patient no.	Age (yr)	Sex	Type	IVSth (mm)	LVPWth (mm)	LVDd (mm)	LVDs (mm)	LVEF (%)	Abnormal findings		
									BMIPP	K mono	FDG
1	50	F	APH	10	11	50	33	63	+	+	+
2	61	M	APH	13	14	48	28	72	+	+	+
3	38	M	ASH	20	12	44	29	66	+	+	+
4	14	M	ASH	15	10	58	31	64	-	-	-
5	62	M	ASH	17	10	45	28	80	+	-	-
6	82	M	ASH	20	12	39	17	73	+	+	-
7	58	M	ASH	22	13	58	26	60	+	+	-
8	46	F	ASH	20	11	41	25	68	+	+	-
9	13	F	ASH	28	11	49	31	76	+	-	-
10	50	M	ASH	15	11	44	25	75	-	-	-
11	17	M	ASH	16	12	47	29	78	+	-	-
12	63	F	ASH	15	11	40	23	74	-	-	-
13	63	F	ASH	18	8	38	22	73	-	-	-
14	60	F	ASH	18	10	41	22	78	+	+	+
15	19	F	ASH	15	8	52	25	71	+	+	+
16	79	M	ASH	15	10	52	30	58	-	-	-
17	53	F	ASH	16	10	43	25	70	+	-	-
18	31	M	ASH	22	12	41	25	75	+	+	np
19	26	F	ASH	15	10	60	41	56	np	-	-
20	24	F	ASH	15	9	51	36	65	np	+	+
21	47	F	ASH	17	12	59	36	62	np	-	-
22	45	M	ASH	16	11	54	37	59	np	+	-
23	14	M	ASH	15	9	38	21	73	np	-	-
24	17	M	ASH	17	12	47	28	60	np	-	-
25	28	M	ASH	15	9	40	30	55	+	np	np
26	58	M	ASH	18	11	40	25	65	+	np	np
27	60	F	ASH	16	10	41	23	74	-	np	np
28	51	M	ASH	22	12	40	22	70	+	np	np

APH = apical hypertrophy; ASH = asymmetrical septal hypertrophy; IVSth = end-diastolic thickness of the septum; LVPWth = end-diastolic thickness of the posterior wall; LVDd = end-diastolic left ventricular dimension; LVDs = end-systolic left ventricular dimension; np = not performed

itself but a fatty acid retention by comparing the data obtained by <sup>11</sup>C palmitate PET studies (36).

### Reduction of BMIPP Uptake in Hypertrophic Cardiomyopathy

BMIPP uptake is reported to be reduced mainly in the hypertrophic myocardium, suggesting abnormal fatty acid metabolism (9-12). In the current study, reduction of BMIPP uptake was also frequently observed. Recent investigations report that defects involving the oxidation of long-chain fatty acids are more likely to cause cardiomyopathy than those involving the metabolism of medium- or short-chain fatty acids (37-43). In addition, another recent report shows that the cardiac hypertrophy is also induced by the suppression of myocardial long-chain fatty acid uptake in rats (44). These results indicate the possible linkage of abnormal long-chain fatty acid uptake with cardiac hypertrophy. The reduced BMIPP uptake observed in patients with HCM may reflect such an abnormal long-chain fatty acid utilization.

### A Variety of Metabolic Patterns

In the current study, there were a variety of metabolic patterns in patients with HCM. A myocardial tissue showing severe impairment of all K mono values, FDG uptake and BMIPP uptake is considered to be fibrotic tissue from the metabolic point of view (Fig. 6). Interestingly, blood flow is preserved in spite of impairment of every metabolic activity. Such a discrepancy between metabolism and blood flow is not usually observed in the ischemic heart disease. Figure 5 shows reduced BMIPP uptake and impaired oxidative metabolism in the hypertrophied myocardium while FDG uptake is preserved,

suggesting that anaerobic glucose metabolism plays a certain part in energy production in these segments. Figure 4 shows that BMIPP uptake is reduced in the segments with relatively preserved K mono values and FDG uptake. In these segments, primary energy source is converted from free fatty acid to

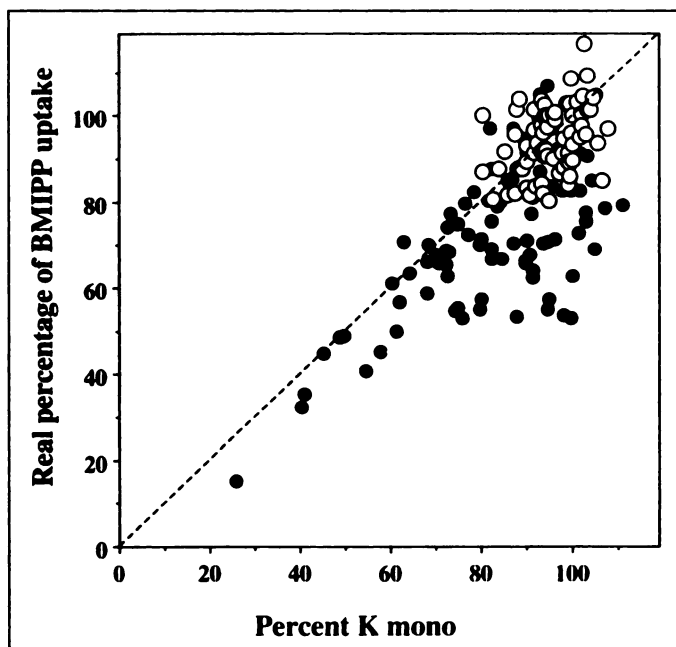


**FIGURE 1.** Correlation between the real percentage of BMIPP uptake and percent K mono in the hypertrophic (filled circles) and nonhypertrophic segments (open circles). The dotted line indicates the line of identity.

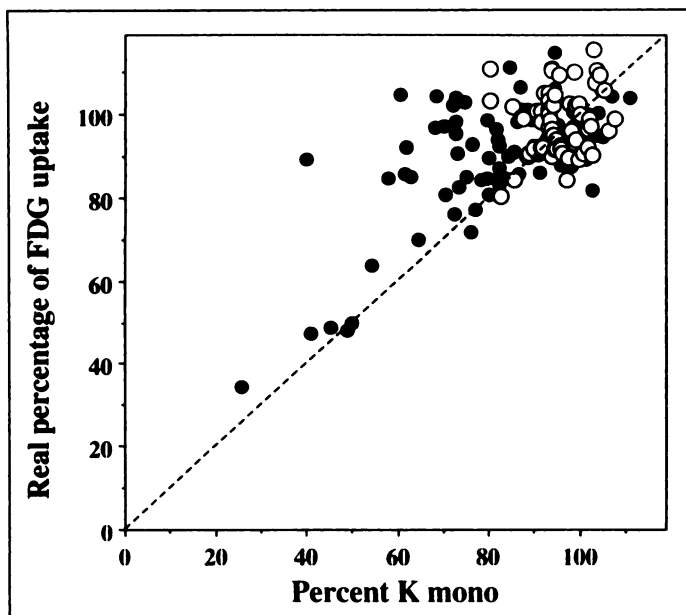


**FIGURE 2.** Correlation between the real percentage of FDG uptake and percent K mono in the hypertrophic (filled circles) and nonhypertrophic segments (open circles). The dotted line indicates the line of identity.

glucose even in the fasting condition. In addition, there were some subjects with preservation of every metabolic parameter in the hypertrophic myocardium (Fig. 3).

#### Relationship Among Metabolic Parameters

Abnormality of BMIPP uptake was more frequently observed and was severer than that of FDG uptake or K mono values in patients with HCM. Figures 1 and 2 and Table 1 showed that BMIPP uptake was more easily impaired than both K mono values and FDG uptake. These data suggest that reduction of BMIPP uptake is the most sensitive parameter of metabolic

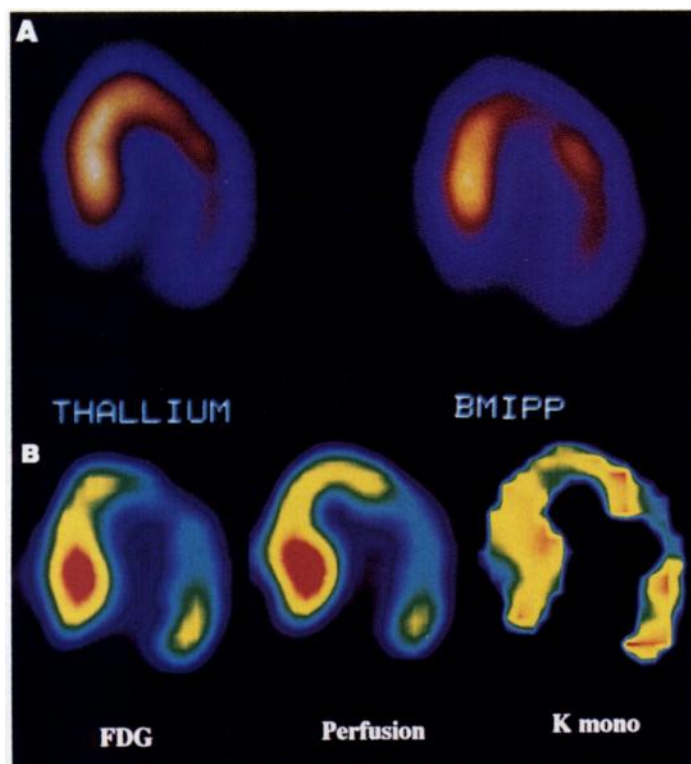


**FIGURE 3.** Horizontal-long axis images of SPECT (A) and PET (B) studies in a patient who had ASH (Patient 13). BMIPP and FDG uptake were maintained, and K mono was also preserved in the hypertrophic septal region.

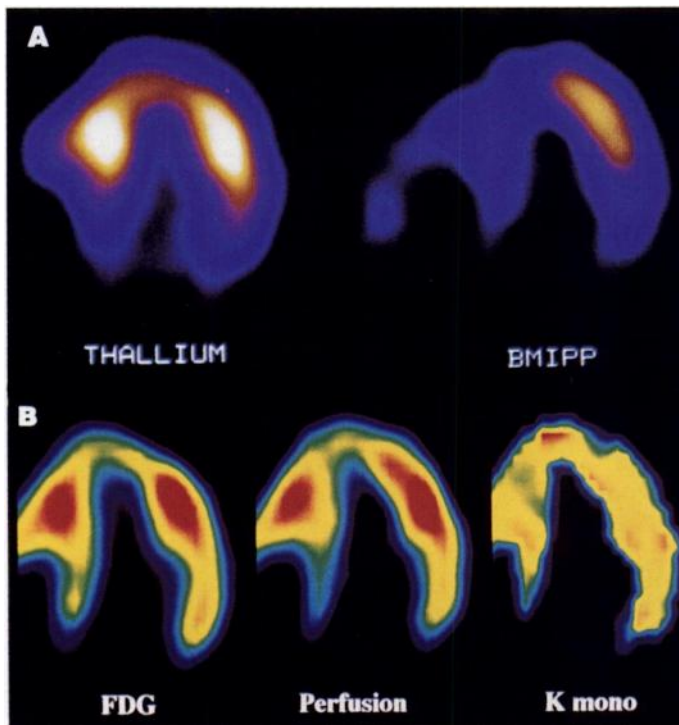


**FIGURE 4.** Horizontal-long axis images of SPECT (A) and PET (B) studies in a patient who had ASH (Patient 11). BMIPP uptake was reduced considerably in the hypertrophied septal region while FDG uptake and K mono were almost maintained.

abnormality observed in HCM. The frequency of abnormality of K mono values was more than that of abnormal findings observed in FDG uptake. Figure 2 indicates that K mono values tend to be more reduced than FDG uptake. Therefore, the first

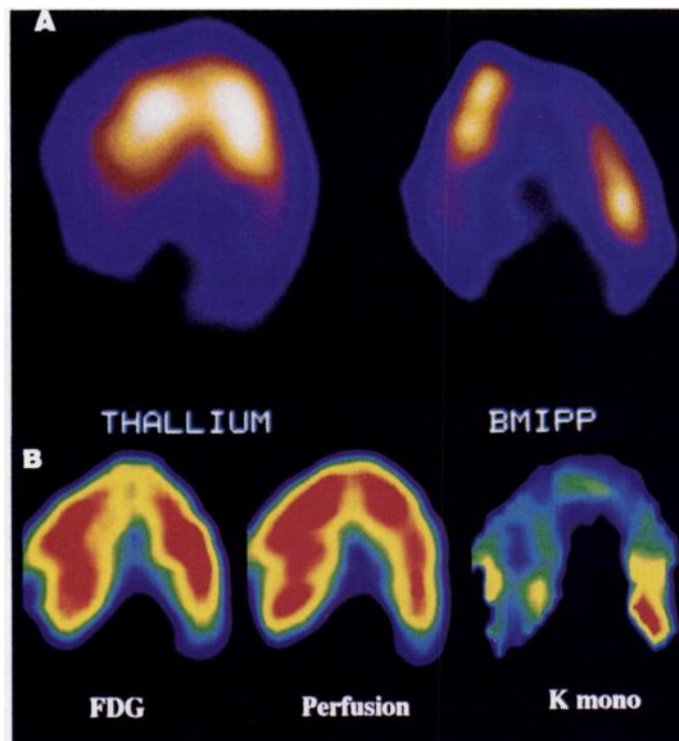


**FIGURE 5.** Horizontal-long axis images of SPECT (A) and PET (B) studies in a patient who had ASH (Patient 8). Hypertrophy was present from the anteroseptal to anterolateral region as shown in the thallium image while apparent BMIPP uptake was relatively homogenous. This indicated that BMIPP uptake was reduced in this hypertrophied region. The K mono image showed that oxidative metabolism was impaired in this hypertrophic region while FDG uptake was almost maintained.

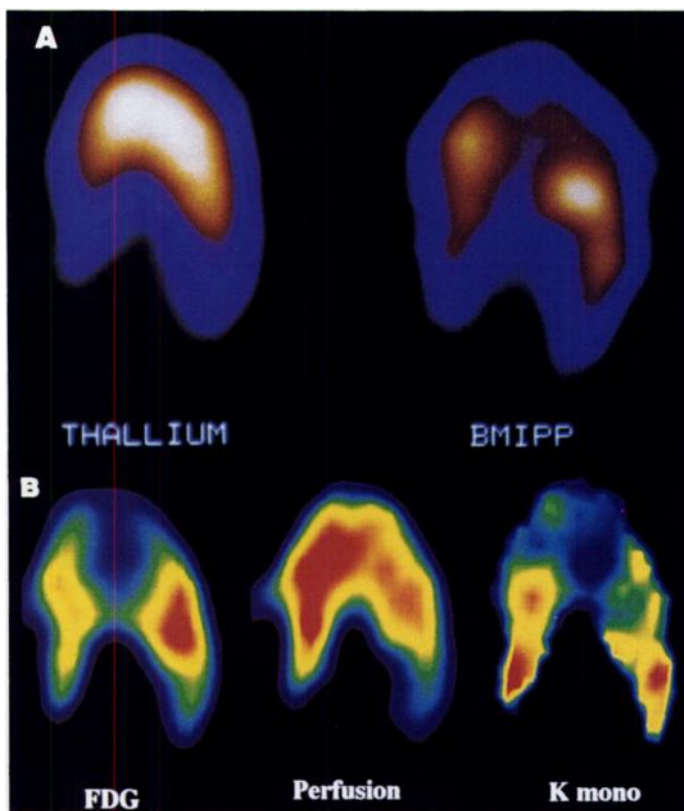


**FIGURE 6.** Horizontal-long axis images of SPECT (A) and PET (B) studies in a patient who had APH (Patient 2). BMIPP and FDG uptake were decreased, and K mono was also reduced in the hypertrophied apical region, indicating impaired metabolic activities while perfusion was preserved.

manifestation of myocardial metabolic abnormalities associated with HCM is considered to be the reduction of BMIPP uptake followed by the impairment of oxidative metabolism, and impaired FDG uptake is thought to be observed only in later stages of the disease.

Such various metabolic abnormalities may indicate the different stages in the course of the disease process. The evaluation of BMIPP uptake, oxidative metabolism assessed with acetate and FDG uptake may contribute to the classification and characterization of the damaged myocardium in patients with HCM. This classification may be helpful for the assessment of the severity and the prediction of the prognosis of this disease. The current observations suggest a wide spectrum of metabolic alterations in this disease. To fully elucidate the abnormality of metabolism in patients with HCM, careful follow-up studies including a wide population are warranted.

#### Study Limitations

In the present studies, we only used semiquantitative data since the main purpose of this study was to compare the PET and SPECT data. SPECT data are usually obtained as semiquantitative ones; thus, in the PET studies, we only used semiquantitative data. For more precise quantitative analysis, comparison of all the PET parameters including  $^{11}\text{C}$  palmitate should be warranted.

Additionally, we normalized every parameter including blood flow, FDG uptake, BMIPP uptake and K mono values to the nonhypertrophic myocardium. This may be another possible limitation of our study. It is based on our assumption that myocardial metabolism is considered to be normal in the nonhypertrophic myocardium and that myocardial blood flow at rest does not differ significantly between hypertrophic and nonhypertrophic myocardium. This may not apply to every

HCM because the etiology of HCM will not be single. A more sophisticated method of partial volume correction (45) and a more refined quantitative analysis of perfusion and metabolism (45–47) may be required in order to overcome this limitation.

#### CONCLUSION

HCM showed a variety of metabolic patterns assessed by PET and SPECT. Our results, however, suggest that the first manifestation of metabolic abnormalities observed in HCM is the reduction of BMIPP uptake followed by the impairment of K mono values and that FDG uptake is reduced finally. Thus, reduction of BMIPP uptake is considered to be the most sensitive indicator of the metabolic abnormalities in patients with HCM.

#### ACKNOWLEDGMENTS

We thank Haruhiro Kitano, BSc, Emiko Komori, RT, and the Cyclotron staff at Kyoto University Hospital for their technical assistance.

#### REFERENCES

- Bing RJ. Cardiac metabolism. *Physiol Rev* 1965;45:171–213.
- Neely JR, Rovetto MJ, Oram JF. Myocardial utilization of carbohydrate and lipids. *Prog Cardiovasc Dis* 1972;15:289–329.
- Neely JR, Morgan HE. Relationship between carbohydrate and lipid metabolism and the energy balance of heart muscle. *Ann Rev Physiol* 1974;36:413–459.
- Opie LH, Owen P, Lubbe W. Estimated glycolytic flux in infarcting heart. *Recent Adv Stud Cardiac Struct Metab* 1975;7:249–255.
- Schelbert HR. Evaluation of “metabolic fingerprints” of myocardial ischemia. *Can J Cardiol* 1986;(suppl A):121A–130A.
- Nishimura T. Approaches to identify and characterize hypertrophic myocardium. *J Nucl Med* 1993;34:1013–1019.
- Sochor H, Schelbert HR, Schwaiger M, et al. Studies of fatty acid metabolism with positron emission tomography in patients with cardiomyopathy. *Eur J Nucl Med* 1986;12:566–569.
- Grover-McKay M, Schwaiger M, Krivokapich J, Perloff JK, Phelps ME, Schelbert HR. Regional myocardial blood flow and metabolism at rest in mildly symptomatic patients with hypertrophic cardiomyopathy. *J Am Coll Cardiol* 1989;13:317–324.
- Kurata C, Kobayashi A, Yamazaki N. Dual tracer autoradiographic study with thallium-201 and radioiodinated fatty acid in cardiomyopathic hamsters. *J Nucl Med* 1989;30:80–87.
- Kurata C, Tawarahara K, Taguchi T, et al. Myocardial emission computed tomography with iodine-123-labeled beta-methyl-branched fatty acid in patients with hypertrophic cardiomyopathy. *J Nucl Med* 1992;33:6–13.
- Takeishi Y, Chiba J, Abe S, Tonooka I, Komatani A, Tomoike H. Heterogenous myocardial distribution of iodine-123 15-(p-iodophenyl)-3-R, S-methylpentadecanoic acid (BMIPP) in patients with hypertrophic cardiomyopathy. *Eur J Nucl Med* 1992;29:775–782.
- Shimonagata T, Nishimura T, Uehara T, et al. Discrepancies between myocardial perfusion and free fatty acid metabolism in patients with hypertrophic cardiomyopathy. *Nucl Med Commun* 1993;14:1005–1013.
- Goodman MM, Kirsch G, Knapp FF Jr. Synthesis and evaluation of radioiodinated terminal p-iodophenyl-substituted  $\alpha$ - and  $\beta$ -methyl-branched fatty acids. *J Med Chem* 1984;27:390–397.
- Knapp FF Jr, Franken P, Kropp J. Cardiac SPECT with iodine-123-labeled fatty acids: evaluation of myocardial viability with BMIPP. *J Nucl Med* 1995;36:1022–1030.
- Tadamura E, Tamaki N, Matsumori A, et al. Myocardial metabolic changes in hypertrophic cardiomyopathy. *J Nucl Med* 1996;37:572–577.
- Maron BJ. Asymmetry in hypertrophic cardiomyopathy. The septal to free wall ratio revisited. *Am J Cardiol* 1985;55:835–858.
- Shapiro LM, McKenna WJ. Distribution of left ventricular hypertrophy in hypertrophic cardiomyopathy: a two-dimensional echocardiographic study. *J Am Coll Cardiol* 1983;2:437–444.
- Sahn DJ, Demaria A, Kisslo J, Weyman A. Recommendation regarding quantitation in M-mode echocardiography: results of a survey of echocardiographic measurements. *Circulation* 1978;58:1072–1083.
- Yamaguchi H, Ishimura T, Nishiyama S, et al. Hypertrophic nonobstructive cardiomyopathy with giant negative T wave (apical hypertrophy): ventriculographic and echocardiographic features in 30 patients. *Am J Cardiol* 1979;44:401–412.
- Maron BJ, Gottidiener JS, Epstein SE. Pattern and significance of distribution of left ventricular hypertrophic cardiomyopathy: a wide angle, two dimensional echocardiographic study of 125 patients. *Am J Cardiol* 1981;48:418–428.
- Nienaber CA, Gambhir SS, Mody FV, et al. Regional myocardial blood flow and glucose utilization in symptomatic patients with hypertrophic cardiomyopathy. *Circulation* 1993;87:1580–1590.
- Tamaki N, Tadamura E, Kawamoto M, et al. Decreased uptake of iodinated branched fatty acid analogue indicates metabolic alterations in ischemic myocardium. *J Nucl Med* 1995;36:1974–1980.
- Takahashi, N, Tamaki, N, Tadamura, E, et al. Combined assessment of regional perfusion and wall motion in patients with coronary artery disease with technetium-99m-tetrofosmin. *J Nucl Cardiol* 1994;1:29–38.

24. Tadamura E, Tamaki N, Yonekura Y, et al. Assessment of coronary vasodilator reserve by N-13 ammonia PET using the microsphere method and Patlak plot analysis. *Ann Nucl Med* 1995;9:109-118.
25. Tadamura E, Tamaki N, Okazawa H, et al. Generator-produced copper-62-PTSM as a myocardial PET perfusion tracer compared with nitrogen-13-ammonia. *J Nucl Med* 1996;37:729-735.
26. Tamaki N, Magata Y, Takahashi N, et al. Oxidative metabolism in the myocardium in normal subjects during dobutamine infusion. *Eur J Nucl Med* 1993;20:231-237.
27. Gropler RJ, Siegel BA, Geltman EM. Myocardial uptake of carbon-11-acetate as an indirect estimate of regional myocardial blood flow. *J Nucl Med* 1991;31:245-251.
28. Brown M, Marshall DR, Sobel BE, Bergmann SR. Delineation of myocardial utilization with carbon-11-labeled acetate. *Circulation* 1987;76:687-696.
29. Ambrecht JJ, Buxton DB, Brunken RC, Phelps ME, Schelbert HR. Regional myocardial oxygen consumption determined non-invasively in humans with [ $^{11}\text{C}$ ] acetate and dynamic positron tomography. *Circulation* 1989;80:863-872.
30. Hata T, Nohara R, Fujita M, et al. Noninvasive assessment of myocardial viability by positron emission tomography with  $^{11}\text{C}$  acetate in patients with old myocardial infarction. Usefulness of low-dose dobutamine infusion. *Circulation* 1996;94:1834-1841.
31. Hoffman EJ, Huang SC, Phelps ME. Quantitation in positron computed tomography: I. Effect of object size. *J Comput Assist Tomogr* 1979;3:299-308.
32. Knapp FF Jr, Ambrose KR, Goodman MM. New radioiodinated methyl-branched fatty acids for cardiac studies. *Eur J Nucl Med* 1986;12:S39-S44.
33. Tamaki N, Kawamoto M, Yonekura Y, et al. Regional metabolic abnormality in relation to perfusion and wall motion in patients with myocardial infarction: assessment with emission tomography using an iodinated branched fatty acid. *J Nucl Med* 1992;33:659-667.
34. Fujibayashi Y, Yonekura Y, Takemura Y, et al. Myocardial accumulation of iodinated beta-methyl-branched fatty acid analogue, iodine-125-15-(p-iodophenyl)-3-(R,S) methyl pentadecanoic acid (BMIPP), in relation to ATP content. *J Nucl Med* 1990;31:1818-1822.
35. Fujibayashi Y, Som P, Yonekura Y, et al. Myocardial accumulation of iodinated beta-methyl-branched fatty acid analogue, iodine-125-15-(p-iodophenyl)-3-(R,S) methyl pentadecanoic acid (BMIPP), and correlation to ATP concentration II. Studies in salt-induced hypertensive rats. *Nucl Med Biol* 1992;2:62-66.
36. Kawamoto, M, Tamaki, N, Yonekura, Y, et al. Significance of myocardial uptake of iodine-123-labeled beta-methyl iodophenyl pentadecanoic acid: comparison with kinetics of carbon-11-labeled palmitate in positron emission tomography. *J Nucl Cardiol* 1994;1:522-528.
37. Kelly DP, Strauss AW. Inherited cardiomyopathies. *N Engl J Med* 1994;330:913-919.
38. Tein I, De Vivo DC, Bierman F, et al. Impaired skin fibroblast carnitine uptake in primary systemic carnitine deficiency manifested by childhood carnitine-responsive cardiomyopathy. *Pediatr Res* 1990;28:247-255.
39. Stanley CA, Hale DE, Berry GT, Deleuw S, Boxer J, Bonnefont J-P. A deficiency of carnitine-acylcarnitine translocase in the inner mitochondrial membrane. *N Engl J Med* 1992;327:19-23.
40. Hug G, Bove KE, Soukup S. Lethal neonatal multiorgan deficiency of carnitine palmitoyltransferase II. *N Engl J Med* 1991;325:1862-1864.
41. Taroni F, Vederio E, Fiorucci S, et al. Molecular characterization of inherited carnitine palmitoyltransferase II deficiency. *Proc Natl Acad Sci USA* 1992;89:8429-8433.
42. Hale DE, Batshaw ML, Coates PM, et al. Long-chain acyl coenzyme A dehydrogenase deficiency: an inherited cause of nonketotic hypoglycemia. *Pediatr Res* 1985;19:666-671.
43. Rocchiccioli F, Wanders RJA, Aubourg P, et al. Deficiency of long-chain 3-hydroxyacyl-CoA dehydrogenase deficiency: a cause of lethal myopathy and cardiomyopathy in early childhood. *Pediatr Res* 1990;28:657-662.
44. Kusaka Y, Tanaka T, Okamoto F, et al. Effect of sulfo-N-succinimidyl palmitate on the rat heart: myocardial long-chain fatty acid uptake and cardiac hypertrophy. *J Mol Cell Cardiol* 1995;27:1605-1612.
45. Iida H, Kanno I, Takahashi A, et al. Measurement of absolute myocardial blood flow with  $\text{H}_2^{15}\text{O}$  and dynamic positron emission tomography. Strategy for quantification in relation to the partial-volume effect. *Circulation* 1988;78:104-115.
46. Bergmann SR, Weinheimer CJ, Markham J, Herrero P. Quantification of myocardial fatty acid metabolism using PET. *J Nucl Med* 1996;37:1723-1730.
47. Iida H, Rhodes CG, Araujo LI, et al. Noninvasive quantification of regional myocardial metabolic rate for oxygen by use of  $^{15}\text{O}_2$  inhalation and positron emission tomography. Theory, error analysis, and application in humans. *Circulation* 1996;94:792-807.

## Perfusion-Contraction Mismatch During Inotropic Stimulation in Hibernating Myocardium

Gianmario Sambuceti, Assuero Giorgetti, Luca Corsiglia, Cecilia Marini, Jan Schneider-Eicke, Claudio Brunelli, Paolo Marzullo, Antonio L'Abbate, Salvatore Capponnetto and Oberdan Parodi  
*Consiglio Nazionale delle Ricerche Institute of Clinical Physiology, Pisa; and Cattedra di Cardiologia, University of Genoa, Genoa, Italy*

The aims of this study were to assess the value of dobutamine echocardiography in identifying myocardial hibernation versus stunning and to elucidate the underlying pathophysiological mechanism of the contractile impairment. **Methods:** Twenty-one patients with isolated stenosis of the left anterior descending artery were evaluated 1 mo after thrombolysed acute anterior infarction. Regional function and blood flow were measured using echocardiography and PET at rest and during dobutamine administration (10  $\mu\text{g}/\text{kg}/\text{min}$ ). **Results:** Defined by [ $^{18}\text{F}$ ]fluorodeoxyglucose uptake, 36 of 102 dyssynergic segments were necrotic, and 66 were viable. The latter segments were subdivided according to their [ $^{13}\text{N}$ ]ammonia flow distribution: 30 hibernating regions with perfusion defects (flow of  $<80\%$  of maximum) and 36 stunned areas with preserved resting perfusion (flow of  $\geq 80\%$  of maximum). Resting flows were similar in necrosis and hibernation ( $0.43 \pm 0.18$  versus  $0.47 \pm 0.16$   $\text{ml}\cdot\text{min}^{-1}\cdot\text{g}^{-1}$ ; not significant), and both resting values were lower than those seen in stunning ( $0.79 \pm 0.24$ ;  $p < 0.05$ ). Flow response to dobutamine was markedly reduced in necrosis (dobutamine/resting flow =  $1.16 \pm 0.27$ ), whereas it was maintained in hibernation ( $1.65 \pm 0.54$ ) and stunning ( $1.42 \pm 0.57$ ). Dobutamine improved function in a higher number of stunned (55%) than hibernating (16%) or necrotic (11%) segments. **Conclusion:** Dobutamine improves

function mainly in stunned myocardium and does not reliably identify hibernation. The lack of functional response in hibernation is not related to an exhausted vasodilating capacity.

**Key Words:** PET; echocardiography; myocardial blood flow; myocardial infarction

*J Nucl Med* 1998; 39:396-402

After thrombolysis for acute myocardial infarction, a residual dysfunction can be observed in the majority of cases. In these patients, the appropriate choice of either conservative or interventional therapy depends on the correct identification of the mechanisms underlying the contractile impairment.

Postinfarction left ventricular dysfunction can arise from myocardial hibernation (1), stunning (2) or necrosis. Myocardial hibernation is defined as chronic wall motion abnormality associated with resting hypoperfusion. Stunning represents a prolonged postischemic dysfunction despite the restoration of a normal or near normal blood flow. In stunning and necrosis, no further interventions are necessary. In the first case, function will recover spontaneously, and the second case represents irreversible damage.

In contrast, the recognition of myocardial hibernation is particularly relevant because it indicates the need for revascu-

Received Jan. 16, 1997; revision accepted May 8, 1997.

For correspondence or reprints contact: Oberdan Parodi, MD, Consiglio Nazionale delle Ricerche Institute of Clinical Physiology, Via P. Savi, 8 I-56100, Pisa, Italy.